Cortical Actomyosin Breakage Triggers Shape Oscillations in Cells and Cell Fragments

Ewa Paluch,*† Matthieu Piel,† Jacques Prost,* Michel Bornens,† and Cécile Sykes*
*Laboratoire Physicochimie "Curie", UMR168 Institut Curie/CNRS, 75231 Paris cedex 05, France; and †Laboratoire Compartimentation et Dynamique Cellulaires, UMR144 Institut Curie/CNRS, 75231 Paris cedex 05, France

ABSTRACT Cell shape and movements rely on complex biochemical pathways that regulate actin, microtubules, and substrate adhesions. Some of these pathways act through altering the cortex contractility. Here we examined cellular systems where contractility is enhanced by disassembly of the microtubules. We found that adherent cells, when detached from their substrate, developed a membrane bulge devoid of detectable actin and myosin. A constriction ring at the base of the bulge oscillated from one side of the cell to the other. The movement was accompanied by sequential redistribution of actin and myosin to the membrane. We observed this oscillatory behavior also in cell fragments of various sizes, providing a simplified, nucleus-free system for biophysical studies. Our observations suggest a mechanism based on active gel dynamics and inspired by symmetry breaking of actin gels growing around beads. The proposed mechanism for breakage of the actomyosin cortex may be used for cell polarization.

INTRODUCTION

Cell division and migration require shape changes in which actin polymerization and myosin motors play a central role. If the mechanisms of actin polymerization and assembly in cell motility have been fairly well characterized with the use of simplified systems (1,2), the understanding of the interplay between motors and the actin network requires further investigations. Also, cells must control their morphology dynamically through complex biochemical and mechanical pathways to ensure proper function. A possible coordinator of the long-distance integration of these various processes is the microtubule (MT) system (3). Indeed, there is a growing body of evidence that, for cell migration, MTs interact with the actomyosin system, for example by reducing its contractility (4–6). Cortex contractility is involved as well in cell division, at least for the definition of the division axis (7) and for mitotic cell rounding (8). As MTs have been shown to regulate actomyosin contractility, possibly due to the Rho-kinase pathway, the spontaneous behavior of the actomyosin cortex in the absence of MTs is thus an important issue in cell dynamics. We address this issue here using both cells and simplified cell systems.

Depolymerization of MTs induces cortical oscillations in cells growing in suspension, like lymphoblasts (9), as well as during spreading of adherent fibroblastic cells (10). Since such oscillations are observed only in situations where adhesion is weak, they may reveal a specific regime of actomyosin dynamics that would be unveiled in the absence of adhesion. We thus developed an experimental setup allowing us to observe oscillations with adherent cells in the absence of MTs under conditions where they could not attach to the substrate. In experiments with lymphoblasts, actin and myosin distributions had been visualized by immunolocalization on fixed cells, a procedure that did not allow for real time characterization (9). Here, the dynamical observation of actin and myosin allowed us to determine that the membrane bulge was first devoid of detectable actin or myosin. This phenomenon was found for entire cells as well as for cell fragments, and the oscillatory behavior was shown to result from actomyosin contractility. Moreover, the ability of cells to oscillate in these conditions correlated positively with their ability to migrate in control conditions. To account for the experimental oscillation phenomenon, we propose a general mechanism based on instability and contraction of the actomyosin gel.

MATERIALS AND METHODS

Cells

Human KE37 (respectively Jurkat) cell line of T-lymphoblastic origin was grown in RPMI 1640 (GIBCO, Invitrogen, Carlsbad, CA) supplemented with 7% (respectively 10%) fetal calf serum (Eurobio, Courbevoie, France). Murine L929 cell line was grown in Dulbecco's modified Eagle's medium (DMEM, GIBCO, Invitrogen) supplemented with 10% fetal calf serum.

Drug treatments

MTs were disrupted with nocodazole (NZ) (Sigma, St. Louis, MO) at 5 μM final concentration. For the lymphoblastic cell lines (KE37 and Jurkat), a treatment at 37°C for 15 min was sufficient. For L929 cells, the NZ treatment was carried out on ice for 1 h; cells were then left to recover at 37°C for 30 min. This treatment depolymerized all the MTs and no reassembly was observed at 37°C (as checked by immunostaining of tubulin).

Myosin II inhibition was achieved using 75 μM blebbistatin (Bb) treatment during 30 min (11) (gift from T. Mitchison, Harvard Medical School, Boston, MA).

Rho-kinase was inhibited by a 2 h treatment with 10 μM Y-27632 (12) (Calbiochem, San Diego, CA).

Submitted February 2, 2005, and accepted for publication April 27, 2005.

Address reprint requests to Cécile Sykes, Tel.: 33-1-423-46790; Fax: 33-1-405-10636; E-mail: cecile.sykes@curie.fr.

Matthieu Piel's present address is Harvard University, Molecular and Cellular Biology Department, Murray Lab, 16 Divinity Ave., Cambridge, MA 02138 USA.

0006-3495/05/07/724/10 $2.00

doi: 10.1529/biophysj.105.060590

To disrupt microfilaments, cells were treated with 2 μg/ml cytochalasin D (CD) (Sigma) or 0.5 μM latrunculin A (LatA).

Local drug delivery

Local drug treatment was carried out using a microinjector (Eppendorf, Hamburg, Germany) mounted on a microscope equipped with a chamber at 37°C. Cells were observed in phase contrast microscopy (Leica, Solms, Germany) using a 40× air objective. The pressure in the micropipette was maintained at 20–100 hPa, and the pipette opening was between 1 and 2 μm. The micropipette was filled with the appropriate drug in cell medium ((DMEM and Hepes, see below) and dextran Texas Red (0.2 mg/ml) as a fluorescent marker. Drug concentrations were 5 μg/ml for CD and 0.5 μM for LatA. There was no drug for the control and flow jet experiments. The pressure exerted by the flow jet on the cell edge was estimated as follows: simple hydrodynamics gives that the pressure at the tip of the micropipette (P_s) depends on the pressure inside the pipette (P_1), the velocity of the fluid in the tip (v), the diameter (ϕ), and the length (l) of the micropipette tip, and the viscosity η of the fluid, $(P_1 - P_S)/l \approx \eta(v/\phi^2)$. If the pressure in the fluid far from the pipette is P_0 and the distance between the micropipette tip and the cell edge is D, we have also $v \approx (D/\eta)(P_S - P_0)$. We thus obtain $P_S - P_0 \approx (\phi^2/Dl)(P_1 - P_0)$. Taking 1 μm for D, 100 μm for l, 100 hPa for P_1, and 1 μm for ϕ, we find that the local pressure exerted on the cell edge, $P_S - P_0$, is of the order of 10^2 Pa.

Polyethyleneglycol (PEG)-coated coverslips

The surface treatment protocol was adapted from (13). Glass coverslips were cleaned with a piranha solution (H_2O_2/H_2SO_4, 30:70 v/v), rinsed twice with ultra-pure water, once with methanol, and incubated overnight in a solution of methanol containing v/v 0.85% of glacial acetic acid, 4.25% of ultra-pure water, and 2.2% of 3-mercaptopropylmethoxysilane (Roth Sochiel, Lauterbourg, France). Coverslips were then rinsed with methanol, dried with argon, heated at 120°C during 5 min, and incubated during 2 h with freshly prepared *m*-PEG-maleimide, molecular weight 5000 (Nektar/Shearwater, San Carlos, CA) at 2 mg/ml in phosphate-buffered saline, pH 7.5. Finally, coverslips were rinsed once with phosphate-buffered saline, twice with ultra-pure water, dried with argon, stocked under vacuum, and used within 10 days.

Cell synchronization

Synchronization of L929 fibroblasts in early G1 phase was accomplished by mitotic shake. Cells were grown to 50% confluence on a collagen-fibronectin coated, 150 cm^2 culture flask; 1 h before the mitotic shake itself, the flask was slightly shaken to remove less adherent cells. Mitotic cells were then collected by a strong shake-off, harvested, and replated on a collagen-fibronectin coated, 25 cm^2 flask to let them perform cytokinesis. After 3 to 4 h, they were treated with NZ on ice, and then prepared for observation. For G2 synchronization, cells were treated with NZ 16h30 after the shake-off, ensuring at least 50% of the cells in the reduced motility phase $<$2.5 h before mitosis (14) (average cell cycle length in our experiments: 17 h).

Preparation of detached L929 cells

Cells were detached with trypsine (GIBCO, Invitrogen), harvested, and resuspended in fresh DMEM with 15 mM Hepes pH 7.2. To keep them in suspension, they were then injected into a chamber made of two PEG coverslips separated by a 165 μm spacer (Gel-Pak, Hayward, CA). This spacer was thin enough to avoid cell dragging by convection flow without constraining the cells. The chamber was sealed with a 1:1:1 w/w mixture of vaseline, lanoline, and solid paraffine.

L929 cell fragments

Cells cultivated on collagen-fibronectin coated plastic plates (Rinzl, Pocketscope.com, Alpharetta, GA) were incubated at 37°C in the presence of 1.5 μg/ml CD for 30 min and of 5 μM NZ for the last 10 min. Cells were then centrifuged at 15,000 × g for 40 min at 37°C in the presence of CD and NZ to pellet nuclei (karyoplasts) and fragments. The pellet was resuspended in fresh DMEM with 5 μM NZ (and no CD). Karyoplasts were separated from fragments by 2 min centrifugation at 120 × g at 37°C. Fragments were then harvested by centrifuging the supernatant at 100,000 × g at 37°C during 20 min. The pellet was resuspended in fresh DMEM with 5 μM NZ and used within a day.

Transfections

The expression plasmid for myosin II regulatory light chain-green fluorescent protein (RLC-GFP) was a gift from Rex Chisholm, Northwestern University, Chicago, IL (T.-L. Chew, W. Wolf, and R. Chisholm, unpublished). The expression plasmid for actin-GFP was a gift from Beat Imhof, University of Geneva, Switzerland (15). L929 cells were transfected by electroporation and seeded on collagen-fibronectin coated plates. Fragments were produced the following day.

Video microscopy

Time-lapse images were taken with a Leica DMIRBE microscope controlled by Metamorph software (Universal Imaging, Downingtown, PA), equipped with a 37°C chamber. The chamber was also controlled at 5% CO_2 for observation in open dishes (KE37, Jurkat, and cell fragments). For observation between sealed PEG coverslips, 15 mM Hepes was used instead. Phase contrast images were acquired using a cooled charge-coupled device camera (Micromax, Roper, Evry, France). For the study of transfected fragments, time-lapse z-sequences were collected with a four-dimensional deconvolution microscope controlled by Metamorph 5.7 software. The system is assembled on a bottom port of an inverted microscope (Leica DM IRB2) placed into an incubator for temperature control at 37°C (Life Imaging Services, Reinach, Switzerland). We used a 100×, 1.4 numerical aperture oil immersion objective and a cooled charge-coupled device detector (Roper Coolsnap HQ). Z-positioning was accomplished by a piezo-electric driver (Physik Instrument, Karlsruhe, Germany) mounted underneath the objective lens. The deconvolution process was achieved using the Metamorph point spread function-based iterative constrained modified Gold algorithm (16), which allows a significant increase in contrast and signal/noise ratio of the data. The sequences were then reconstructed in three dimensions using the maximum intensity projection algorithm. Photobleaching experiments were carried out with a Zeiss (Oberkochen, Germany) confocal microscope controlled by LSM 510 META. We used a 63×, 1.4 numerical aperture oil immersion, Plan-Apochromat objective and an ion argon, 25 mW, laser (488 nm). Image contrast was reprocessed using Metamorph software.

RESULTS

Nocodazole-treated L929 fibroblasts form a constriction ring that moves back and forth across the cell

When cultured on plastic, L929 fibroblasts display a lamellipodium oriented toward the direction of cell migration. Depolymerization of MTs with nocodazole (NZ) treatment induces lamellipodial membrane protrusions all along the periphery of the cell (17) and increases actomyosin contractility (4).

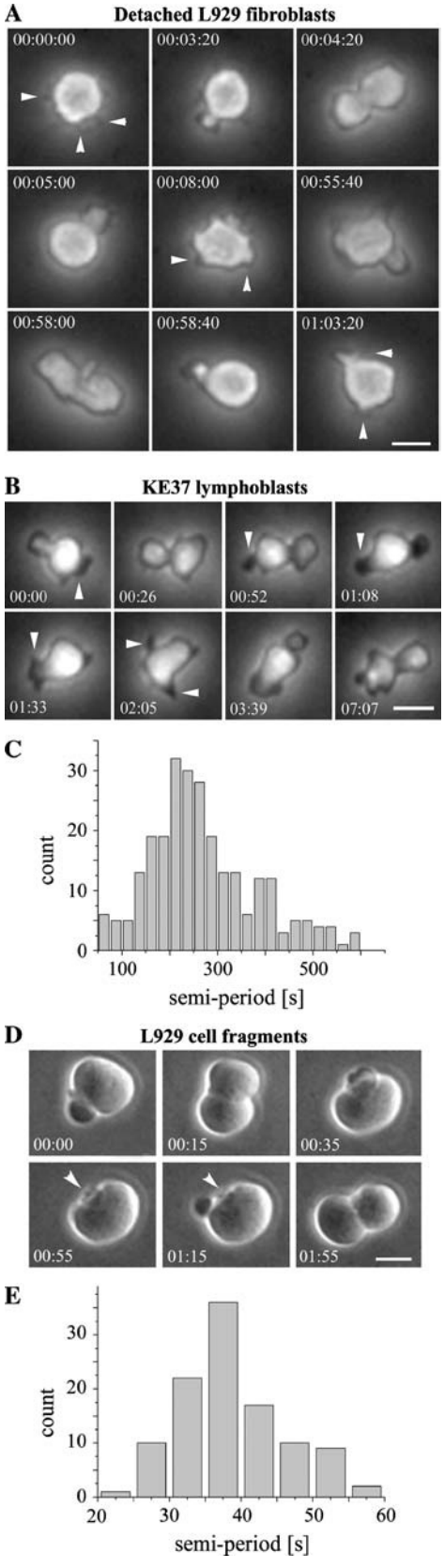

FIGURE 1 Oscillatory behavior of cells and cell fragments. (*A* and *B*) Successive phase-contrast images (20× objective) of (*A*) detached L929 fibroblasts and (*B*) KE37 lymphocytes. Cells are treated with NZ. (Scale bars, 10 μm). White arrowheads indicate membrane protrusions. (*A*) Time in h/min/s. Note that the cell has turned between frames 00:08:00 and 00:55:40; (*B*) Time in min/s. (*C*) Semiperiod of the oscillation in KE37 cells (265 crossings of the ring in a total of 38 oscillating cells from the same experiment). The mean semiperiod here is 284 s, yet varies from one experiment to the other. Semiperiods above 650 s are not displayed, being considered as pauses. (*D*) Successive phase contrast images of a L929 fragment (100× objective). Time in min/s. White arrowheads, disappearance of the ring (00:55). Interestingly, the new ring is formed close to this point (01:15). (Scale bar, 5 μm). (*E*) Semiperiod of the oscillation measured for one L929 fragment during 2 h (107 ring crossings). The mean period is 36.8 s. Semiperiods above 60 s are not shown, being considered as pauses.

L929 fibroblasts treated with NZ, and then detached by trypsinization, could be observed for up to 6 h on PEG-grafted coverslips that prevented cells from adhering (see Materials and Methods). Once detached, cells first remained round, and an oscillatory behavior started after 45 min to 3 h. A representative example is displayed in Fig. 1 *A*: a constriction ring formed and crossed the cell body. Once the ring had reached the opposite side of the cell, a small knob remained, and important membrane activity was displayed by the main cell body. Eventually, the ring moved back across the cell and usually resorbed. Such back and forth movements occurred repeatedly, separated by pauses of variable length. There was no well-defined period, the timescales varying from one cycle to the other.

The oscillatory behavior was observed in up to 37% of non-synchronized cells. This number was increased to 87% when cells were previously synchronized in the postmitotic G1 phase. Conversely, only 28% of cells synchronized in the late G2 phase oscillated. From motility experiments, it is known that cells display a more active migration in the G1 phase than at the end of the G2 phase (14). Therefore, the ability of cells to oscillate coincides with their ability to migrate.

The oscillatory behavior of L929 cells was comparable to the oscillations observed in the absence of MTs in KE37 lymphoblastic cells, which grow in suspension (9) (Fig. 1 *B* and Supplementary Movie 1), or in Jurkat cells, another human lymphoblastic cell line (data not shown). However, KE37 displayed a more regular behavior where a semiperiod (time measured between two crossings of the ring at the middle of the cell) could be defined (Fig. 1 *C*). In both L929 and KE37 cells, once the constriction ring had reached one end of the cell, the other end displayed accentuated membrane activity (*white arrowheads* in Fig. 1 *A* at 08:00, and in Fig. 1 *B*) and lamellipodia formation (Fig. S1). The displacement velocity of the ring during its movement across the cell was ~5–10 μm/min in KE37 as well as in L929.

Depolymerization of MTs thus induces a similar oscillatory behavior in lymphoblasts and detached fibroblasts. This behavior is spontaneous and lasts for at least 6 h, suggesting that it is governed by an intrinsic and general cellular mechanism. We therefore wondered whether it would be

conserved in a simplified, nucleus-free system, such as those previously used for migration studies (18–20).

Cell fragments oscillate

Cell fragments from 0.5 to 10 μm in diameter were obtained as a side product of L929 fibroblast enucleation using a protocol adapted from Prescott et al. (21) (see Materials and Methods). A great number of cell fragments was produced, possibly by pearling of the membrane tube formed between the cell and the nucleus pulled off by the centrifugation, or due to the fragility of the cell cortex. Fragments from 3 to 10 μm in diameter were observed by video microscopy.

When resuspended in fresh medium supplemented with NZ, fragments remained in suspension, and 70–80% displayed an oscillatory behavior that persisted for at least 8 h. A representative sequence is displayed in Fig. 1 *D*. The constriction ring oscillated very smoothly. A remarkable difference with entire cells was that no membrane protrusion activity was observed (Fig. 1 *D*, Supplementary Movie 1). This could be related to the small size of the fragments. For a given fragment, a semiperiod was well defined (Fig. 1 *E*), but varied from one fragment to the other (from 30 to 150 s) with no clear correlation with size, probably due to the inhomogeneity in fragment composition. The velocity of the ring movement was ~5–10 μm/min, comparable to the values observed for entire cells. The oscillatory behavior can thus be generalized to cell fragments.

Oscillations depend on actin polymerization and myosin II activity

We then investigated how actin and myosin II were involved using both L929 cell fragments and KE37 cells. Cytochalasin D (CD) was used to inhibit actin dynamics. In cells and cell fragments first treated with CD for 30 min, the addition of NZ did not result in ring formation. Adding CD to already oscillating NZ-treated KE37 cells or L929 fragments stopped the oscillatory behavior in <5 min. Strikingly, once the oscillation had stopped, the constriction slowly relaxed during 10–30 min (data not shown). Treatment of oscillating cells with 0.5 μM latrunculin A (LatA) gave the same result, which suggests that actin is either more concentrated or less dynamic at the constriction. We characterized the effect of low amounts of CD on the well-defined semiperiod of KE37 cells: increasing CD concentration decreased the number of oscillating cells and increased the semiperiod (Fig. 2, *A* and *B*).

We inhibited myosin II using blebbistatin (Bb) (11). If we first added Bb, the addition of NZ did not induce oscillation. If Bb was added to NZ-treated cells once they had formed an oscillating ring, the oscillation stopped after 15–30 min, and a large lamellipodium formed that resembled that of control cells (Supplementary Movie 2). No constriction was

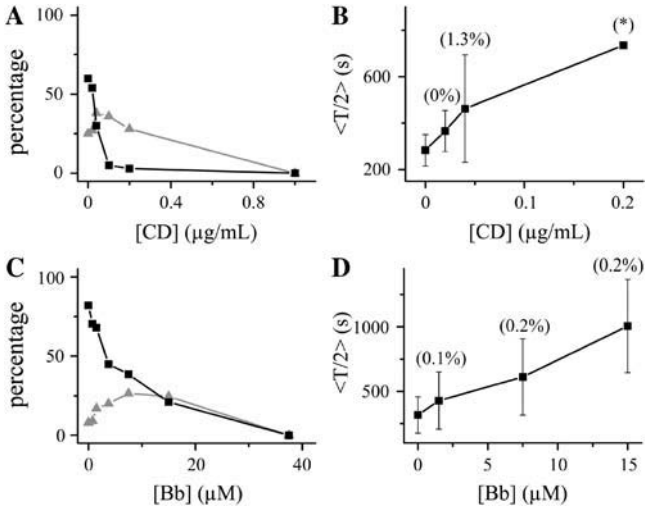

FIGURE 2 Effects of increasing quantities of CD (*A* and *B*) and Bb (*C* and *D*) on oscillating, NZ-treated KE37 cells. (*A* and *C*) Percentage of oscillating cells (*squares*) as a function of the concentration of CD (*A*) or Bb (*C*). Triangles correspond to cells that could not be classified. The slight increase at intermediate concentrations denotes an increased number of cells in a transient state. (*B* and *D*) Corresponding mean semiperiod of the oscillation, $\langle T/2 \rangle$, as a function of the concentration of CD (*B*) or Bb (*D*). The error bars correspond to standard deviations. The numbers in parentheses give the *p*-value: the probability that the calculated $\langle T/2 \rangle$ is different from the previous one by chance alone. Consecutive data points are significantly different (*p*-value $< 1.5\%$). In *B*, for [CD] > 0.05 μg /mL, since very few cells oscillated, $\langle T/2 \rangle$ could be properly measured for only one oscillation cycle (*).

observed, demonstrating that the ring formation depends on myosin II contractile activity. If Bb was then removed by rinsing the cells, the oscillatory behavior resumed after 30 min. Similar results were obtained with L929 cell fragments, although no lamellipodium was observed. In lymphoblastic cells, the effect of gradual Bb addition was comparable to that of CD (Fig. 2, *C* and *D*).

Using an alternative approach to affect myosin II activity through the Rho pathway that enhances contractility, we checked that a Rho-kinase inhibitor, Y-27632 (12), stopped the oscillation in NZ-treated KE37 cells. No oscillatory behavior was observed when cells were treated with Y-27632 before NZ addition. From these experiments, we conclude that the oscillatory behavior depends on actin polymerization and myosin II activity, which prompted us to investigate their dynamics.

Dynamics of actin and myosin II in oscillating fragments

To obtain a dynamic characterization of the oscillation mechanism, we produced fragments from L929 cells expressing either actin-GFP (15) or myosin II regulatory light chain (RLC)-GFP, which can be used as a reporter for myosin II (T.-L. Chew, W. Wolf and R. Chisholm, unpublished). The small size of the cell fragments allowed

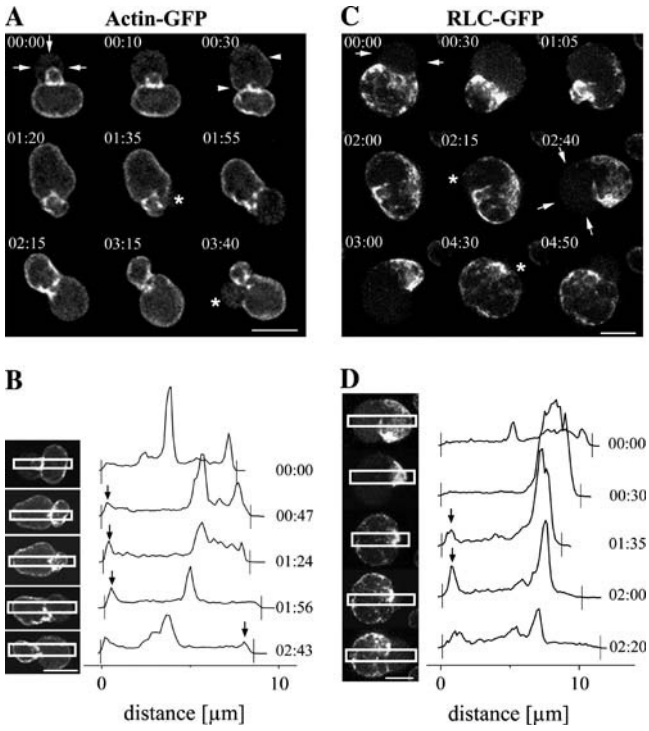

FIGURE 3 Analysis of actin and myosin II distributions in oscillating L929 fragments. Images are selected frames from deconvolved time-lapse *z*-sequences (Supplementary Movies 3 and 4) reconstructed in three dimensions (see Materials and Methods). Examples of stacks of deconvolved scans can be seen in Supplementary Movie 6. (*A* and *C*) Successive images of an L929 fragment transfected with actin-GFP (*A*) or RLC-GFP (*C*). Image contrast (including γ) has been adjusted with Metamorph Software. Time in min/s. White arrows indicate the growing parts of the fragments. White asterisks mark holes formed in the actomyosin shell, through which the bulge will be expelled. White arrowheads in *A* point out brighter regions where actin is progressively recruited to the cortex. (*B* and *D*) Fluorescence profile analysis of, respectively, *A* and *C* time-lapse. For each frame, the fluorescence intensity of actin and myosin II is plotted (line scan) as a function of the distance along the oscillation axis. Each line scan is performed on a line of 10-pixel width (*white rectangles* on the images). Vertical lines on the graphs correspond to the positions of the fragment membrane inside the white rectangles. Time in min/s. (*B*) 00:00, actin is present at the ring (maximum peak) and at the right-hand side part of the membrane (smaller peak). As the ring goes to the right (the two peaks get closer together), actin appears at the left-hand part of the membrane and accumulates over time (*black arrows*). Between 01:24 and 01:56, the ring starts its movement to the left and a bulge devoid of detectable actin grows (no peak in the *right part* of the graph). When the ring gets closer to the left-hand side, a new peak of actin starts growing on the right (*black arrow*). (*D*) 00:00, myosin II is present at the ring area and at the right-hand side part of the membrane. When the ring reaches this point (fusion of the two peaks), there is still no apparent myosin in the left-hand side of the fragment. 01:35, myosin is redistributed to the entire membrane (*black arrow*). Then myosin II accumulates at the membrane and a bulge devoid of detectable myosin grows on the right. (Scale bars, 5 μm.)

us to acquire time-lapse *z*-sequences and several oscillations could be recorded without bleaching.

Representative dynamic distributions of actin and myosin II in oscillating fragments are displayed in Fig. 3 and Supplementary Movies 3 and 4 (see Fig. S2 for other examples). Fluorescence profile analysis was performed on deconvolved time-lapse images (Fig. 3, *B* and *D*). Actin was essentially located at the membrane throughout the experiment (Fig. 3 *B*), but its distribution varied significantly during the oscillation cycle. Strikingly, the growing bulge surface was first devoid of detectable actin in comparison with the shrinking part of the fragment (Fig. 3 *A* at 00:00). Then actin was gradually recruited to the plasma membrane of the bulge (Fig. 3 *A*, *white arrowheads*) until the distribution became uniform all over the surface (Fig. 3 *A* at 01:20). After a delay, a new bulge was expelled through a hole that formed in the actin shell (Fig. 3 *A*, *white asterisks*). This hole was rimmed with actin (Fig. S2 *C* and Supplementary Movie 6). The new bulge was, in turn, initially devoid of detectable actin. In general, the new bulge nucleated next to where the previous bulge had collapsed. Bulge formation was reminiscent of blebbing (22–24), but here, the bulge size rapidly reached the size of the cell or cell fragment.

The dynamics of myosin II were similar to those of actin yet led to a more patchy distribution (Fig. 3, *C* and *D*, Supplementary Movie 4). Strikingly, myosin II recruitment to the growing bulge started later than for actin. For fragments oscillating with a semiperiod between 100 and 120 s, the delay was on average 50 s (measured for 10 oscillation cycles on 4 fragments). Importantly, a new bulge formed only when both myosin II and actin had respread to the entire membrane. Similar dynamics of actin and myosin II were observed in entire L929 cells (Fig. S3, Supplementary Movie 5).

From these observations, we conclude that 1), hole formation in the actomyosin cortex triggers bulge growth, and 2), the oscillatory behavior is driven by rapid redistributions of cortical actin and myosin II.

Osmotic swelling suppresses the oscillation

To figure out whether or not hole formation could by induced be hydrostatic pressure effect on the cortex (22), we first investigated the effect of increased internal pressure on the oscillation by performing osmotic swelling experiments. Adding different amounts of water (5–50% water in the medium) (25) to already oscillating KE37 cells drastically reduced the number of oscillating cells (Fig. 4 *A*). Thus, oscillation is not facilitated by increasing the internal pressure, an observation that does not favor the hypothesis of bulging induced by hydrostatic pressure alone.

Local cortex alteration induces bulging

We then wondered whether the membrane bulging that triggers the oscillation could occur where the cortex is altered; we used a micropipette system either to deliver locally CD or LatA or to act mechanically with the expelled jet. To prevent cells from being dragged by the flow, L929 cells were treated

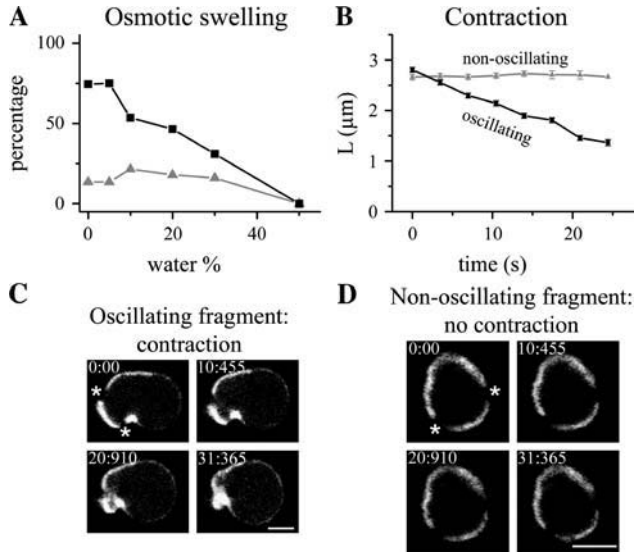

FIGURE 4 Osmotic pressure and photobleaching experiments. (*A*) Percentage of oscillating KE37 NZ-treated cells (*square symbols*) as a function of the percentage of pure water added to the RPMI medium. Triangles correspond to cells that could not be classified. The slight increase of unclassifiable cells at intermediate concentrations denotes an increased number of cells in a transient state. (*B–D*) Photobleaching experiments on actin-GFP transfected fragments. (*C* and *D*) Time-lapse images of the fragments after photobleaching a line (*asterisks*). (Scale bars, 5 μm.) (*B*) Cortex length L between the two bleached spots (*white asterisks* on *C* and *D*) for the oscillating fragment displayed in *C* and the control nonoscillating fragment displayed in *D*. The shrinkage measurement was performed on 10 different fragments. The mean shrinkage velocities ranged from 1.0 to 9.1 μm/min depending on the fragment, and is 3.5 μm/min for the fragment displayed on *B*.

with NZ but maintained weakly adherent (no trypsin treatment). We chose to observe the behavior of nearly spherical cells, which are the closest to detached cells. For CD treatment, the micropipette tip was located at a minimal distance of 7 μm from the cell. In these conditions, local delivery of CD was able to generate a membrane bulge where the drug was delivered in 8 out of 12 cells (Fig. 5); 3 cells produced several bulges instantaneously at different locations on their surface, and 1 cell did not form any bulge. In similar conditions, local application of LatA resulted in the generation of a bulge where the drug was delivered in 7 out of 11 cells; 3 cells produced a bulge elsewhere and 1 cell did not form any bulge (Fig. 5). Local delivery of culture medium alone did not induce bulge formation in the same conditions (Fig. 5). The bulge remained at least 5 min after the drug delivery was stopped, indicating that the cortex breakage persisted. Membrane bulging was never followed by an oscillation cycle. This is probably due to the cell attachment to the substrate, which increases membrane tension and may therefore limit bulge growth.

We tested whether contractility was necessary for bulge formation by locally applying LatA on cells treated beforehand with Bb and did not observe bulge formation (9 cells, Fig. 5). This experiment shows that intracellular pressure alone cannot drive bulge growth, and that myosin II-based contractility is necessary.

More strikingly, the direct effect of tension could be tested by imposing a local mechanical stress. This was achieved by flowing a jet of culture medium on the cell membrane with the pipette tip at a distance of 1–2 μm from the membrane. The local pressure that was exerted on the cell membrane was then of the order of 10^2 Pa (see Materials and Methods). This is slightly below the value of the elastic modulus of an actin gel (26), and also of the critical stress at which symmetry breaks in an actin gel under tension around beads (2), and corresponds to a force of 0.1 nN on a 1 μm^2 surface. Thus this pertubation could be sufficient to induce local rupture of the actin cortex. Notably, although the jet pressed on the membrane, its action did not provoke any invagination, but conversely resulted in the appearance of a membrane bulge in 11 out of 12 cells (1 cell did not form any bulge) (Fig. 5). This experiment favors the idea that a higher local stress can induce cortex breakage.

Photobleaching experiments reveal cortical contraction

Whereas the new bulge grew, the remaining part of the cell or fragment shrank. This could be due to the dynamics of the actomyosin cortex either by actin depolymerization only, or by cortical contraction. To address this issue, we photobleached two spots in the actin cortex of oscillating actin-GFP transfected fragments. We observed reproducibly (10 fragments) that the distance between the two spots decreased, whereas it remained constant in control nonoscillating fragments (Fig. 4, *B–D*). This result provides clear evidence for actomyosin cortical contraction.

DISCUSSION

The above observations support the idea of a common generic oscillatory phenomenon, which we describe below.

Mechanism of the actomyosin cortex breakage

Notably, the first step of the oscillation is the formation of a hole in the actomyosin cortex (Fig. 3, Fig. S2, Supplementary Movies 3 and 4), reminiscent of ''fenestration'' in Walker-carcinoma cells, which has been proposed to result from hydrostatic pressure (22). However, our experiments favor a contractile effect (see Figs. 4 and 5). We thus propose another mechanism, based on cortical contraction only, inspired by studies on actin gels under tension. Indeed, the actomyosin cortex is a highly dynamic cross-linked gel (27) organized as a shell of actin associated with the membrane and maintained under tension by the presence

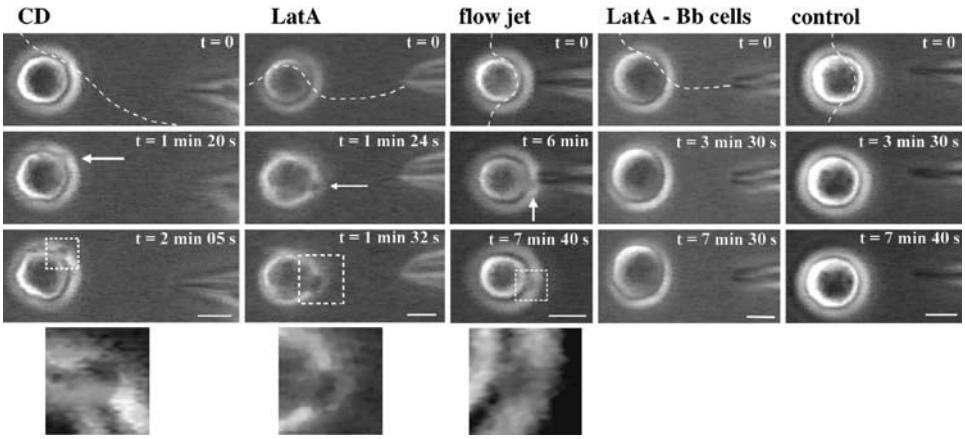

FIGURE 5 Experiments of local bulge induction with CD and LatA delivery, local flow jet, and controls. Each type of experiment has been reproduced on at least 10 cells. The white dashed lines represent the profile of the flow, as visualized using dextran Texas Red as a marker. This profile remained stationary over the time course of the experiment. Local herniation of the membrane is observed for CD and LatA delivery, and mechanical effect induced by the flow jet. No membrane deformation is observed in control experiments where LatA is delivered on Bb treated cells or where the pipette is filled with medium alone. Images on the bottom are zooms of the bulges and correspond to the dashed white selections. Images have been filtered using Metamorph Median Filter function. Scale bars, 10 μm.

of myosin II. A similar actin gel under tension forms around beads that activate actin polymerization. We showed elsewhere that when actin monomers assemble at the surface of these beads, their insertion deforms the existing actin gel, leading to a tension due only to geometry (28). This state precedes symmetry breaking and movement of beads mimicking *Listeria* motility (2,29,30). The same analysis applies here: in the stationary regime of oscillating fragments, the shell is locally under a tension, due here to the activity of myosin II. As long as the shell is closed, the tension $\boldsymbol{T}$, tangential to the cortex (Fig. 6 *A*, *a*), keeps a uniform modulus around the shell, given by the formula

$$\|T\| = \int_{r_{\text{in}}}^{r_{\text{out}}} \sigma_{\tan}(r)dr,$$

where r_{in} and r_{out} are, respectively, the internal and the external radius delimiting the actomyosin gel, and $\sigma_{\tan}(r)$ is the local tangential stress distribution through the gel thickness. The gel thickness $(r_{\text{out}} - r_{\text{in}})$ varies locally due to fluctuations, but the tension remains uniform. From the above formula, we see that where the gel is thinner, the local tangential stress is higher, and can provoke gel rupture or depolymerization. Note that the same effect can be produced by any spatial inhomogeneity in the stress like, for example,

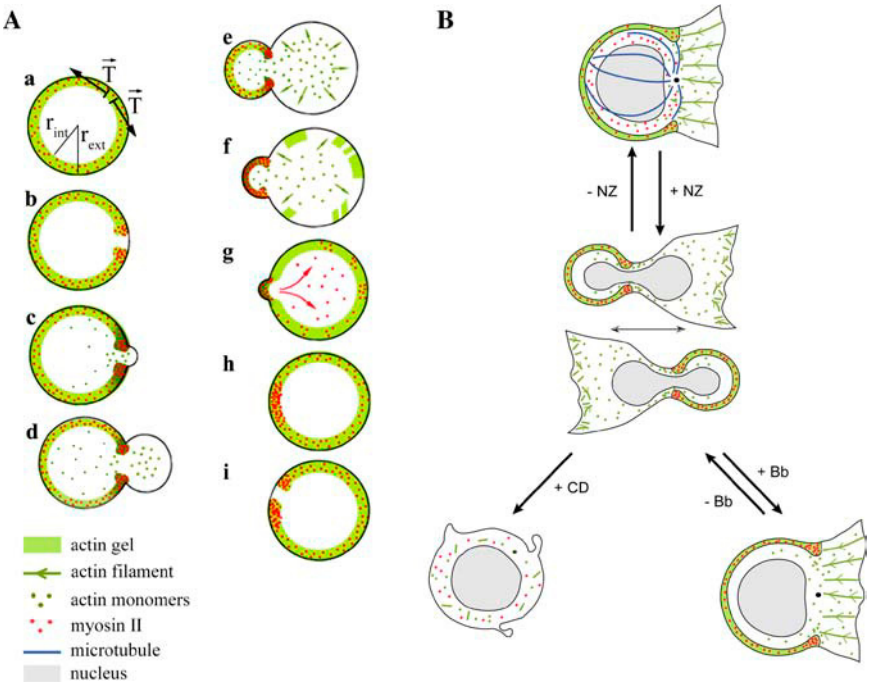

FIGURE 6 Mechanism of the oscillation and perspectives for cell polarity. (*A*, *a–i*) Successive stages of the oscillation. Green arrows indicate actin redistribution to the cortex and red arrows indicate myosin II flux. (*a*) $\boldsymbol{T}$: tension exerted by the actomyosin cortex (see discussion). (*B*) In KE37 control cell (*top cartoon*), myosin II is present at the cell cortex and in the cytoplasm. The addition of NZ provokes cell oscillation. The cartoon corresponds to the situation described for fragments in (*A, f*), when actin starts repolymerizing at the membrane of the growing bulge, which in cells leads to the formation of a lamellipodium. Subsequent addition of Bb stops the oscillation and the cell recovers a control. NZ and Bb treatments are reversible. When treated with CD after NZ, the cell assumes a round shape with small membrane protrusions. This treatment is not reversible.

one caused by a higher local concentration of myosin, as we briefly discuss in the following paragraph. This mechanism is confirmed by the local herniation of the cell membrane at the point where the actin cortex is fragilized either by CD or LatA, or by a mechanical effect (Fig. 5).

A mechanism for the oscillation

Once the hole is formed, the bulge growth could be a priori driven by osmotic pressure, or by contraction. If the bulge growth were osmotically driven, it should be accelerated by a decrease in external osmolarity, which is not what we observe experimentally (Fig. 4 *A*). We therefore propose a model based on contraction, in agreement with the photobleaching and local LatA delivery experiments: after gel rupture, hole formation promotes accumulation of a rim of actomyosin gel (Fig. 6 *A*, *b*), as observed experimentally (Supplementary Movie 6 and Fig. S2 *C*), leaving a portion of membrane devoid of actin and myosin II. The open shell then contracts, as revealed by photobleaching experiments, and this contractility depends directly on both actin and myosin activities, since the oscillation is slowed down when their activity is gradually decreased. Whereas myosin remains linked to the shrinking actin shell, the cytoplasm is extruded through the cortical hole and the growing bulge becomes enriched in actin monomers or short polymers. This enrichment could be induced by solation, i.e., gel disassembly (31), as proposed to explain actin depolymerization at the base of the lamellipodium (32,33). In the bulging part, actin is progressively recruited to the membrane, and a new shell forms (Fig. 6 *A*, *e* and *f*). Polymerization starts at several points, accounting for the irregular aspect of actin at early stages. Then myosin II redistributes to the entire fragment membrane (Fig. 6 *A*, *g*) after a significant delay that is explained by the need of a substrate (the actin network) for the motors to attach. However, a higher concentration of myosin II remains where the constriction movement ended, thus creating a local inhomogeneity in the stress. This inhomogeneity will in turn favor new breakage and bulge growth close by, which is what we observe in most cases (although not all, since a probability remains that the cortex breaks elsewhere). The same mechanism can account for the oscillatory behavior of entire cells, where the progressive recruitment of actin to the bulging side (Fig. 6 *A, e* and *f*) would result in the formation of a lamellipodium (Fig. S1).

Physiological relevance of the oscillation phenomenon

The oscillation phenomenon underlines an intrinsic instability of the cortical actomyosin system. Revealed in artificial conditions, where MTs are depolymerized, this mechanism could be involved in the dynamics of the cell shape, although in usual conditions it is controlled partially or totally by the MT system, likely through the Rho pathway. However, there are situations in which the cell will take advantage of this cortical phenomenon. One clear case of cortically driven instability appears to be the onset of fertilization of the *Caenorhabditis elegans* egg. Indeed, it has been recently observed that the sperm entry triggers a retraction of the cell actomyosin cortex, thus leaving a membrane area free of cortical actin and myosin (34). In this work, the authors show that the cortical flow relies on myosin-based contraction and is triggered by local, centrosome-mediated, release of contractility. Moreover, the velocity at which the cortex contracts in *C. elegans* is in the 1–7 μm/min range, like in our experiments where the cortex shrinks at a velocity of 1–9 μm/min (Fig. 4 *B*). Taken together, these experiments support the mechanism of instability leading to global cortical flows we propose in this work. As asymmetrical division then happens, the *C. elegans* egg must prevent cortical oscillation for proper development, a feature that is possibly achieved by PAR family proteins, which stabilize the asymmetry as suggested by experimental observations (34). More generally, in mitosis, the orientation of the mitotic spindle is altered in dividing cells where Rho is overexpressed, due to enhanced contractility (7). The definition of the division axis in such highly contractile cells could result partly from a spontaneous cortex breakage similar to what we observe.

In the case of cell migration, although lamellipodium extension is often studied as a mechanism autonomously defining polarity, there might be a correlation between cortical actomyosin contractility and the sites where membrane extension is nucleated (35). A possible scenario is that actin and myosin confer active gel properties (36) to the cell cortex producing physical effects that result in membrane extension.

In keeping with these lines, our mechanism of cortex instability could also explain the formation of a lamellipodium in lymphoblast cells, growing in suspension. The shape of the cell body could be that of an actin shell with a stabilized opening through which the cytoplasm is extruded, allowing actin to repolymerize in the bulge that could then become a lamellipodium (Fig. 6 *B*). Indeed, polymerization of actin at such membrane bulging zones can, under certain conditions, transform into lamellipodia (23,37). The presence of MTs, which reduces the recruitment of myosin II to the cortex, tones down cell contractility (6,38–40). The low contractility of the actomyosin shell might then prevent the oscillation dynamics to take place. The stabilized shape would be a round cell body with a constriction at the base of the lamellipodium, as generally observed. Significantly, oscillating NZ-treated cells recovered after Bb addition a shape similar to that of control cells, with a lamellipodium and round cell body (Supplementary Movie 2). Due to Bb treatment, the contractility of the actomyosin shell is reduced, which could explain the stability of the lamellipodium, just like in control cells with MTs.

CONCLUSION

To conclude, our work reveals a spontaneous behavior of membrane bulging under the effect of actomyosin contraction in cellular systems. This behavior was observed in different cell lines, and in cell fragments, a simplified system that paves the way for further biomimetic studies. A physical analysis of our experiments allowed us to propose an innovative mechanism for nucleation and growth of the membrane bulge, based purely on contractility. This mechanism could be used by cells in various processes requiring symmetry breaking and polarization, like in cell migration or in cell division.

SUPPLEMENTARY MATERIAL

An online supplement to this article can be found by visiting BJ Online at http://www.biophysj.org.

We thank J.-B. Sibarita for deconvolution and help with video microscopy; R. Chisholm and B. Imhof for their generous gift of GFP constructs; D. Roche for help with cell synchronization; E. Coudrier, V. Doye, and J. Plastino for critical reading of the manuscript; and F. Jülicher, J.-F. Joanny, and K. Kruse for fruitful discussions. We thank an anonymous reviewer for suggesting to test experimentally the herniation.

This work has been supported by Centre National de la Recherche Scientifique grants (Action concertée Dynamique et Réactivité des Assemblages Biologiques) and by a grant from the Institut Curie (Programme Incitatif et Coopératif). E. P. is supported by a La Ligue contre le Cancer fellowship.

REFERENCES

1. Theriot, J. A., T. J. Mitchison, L. G. Tilney, and D. A. Portnoy. 1992. The rate of actin-based motility of intracellular *Listeria monocytogenes* equals the rate of actin polymerization. *Nature.* 357:257–260.
2. Bernheim-Groswasser, A., S. Wiesner, R. M. Golsteyn, M.-F. Carlier, and C. Sykes. 2002. The dynamics of actin-based motility depend on surface parameters. *Nature.* 417:308–311.
3. Small, J. V., B. Geiger, I. Kaverina, and A. Bershadsky. 2002. How do microtubules guide migrating cells? *Nat. Rev. Mol. Cell Biol.* 3:957–964.
4. Danowski, B. A. 1989. Fibroblast contractility and actin organization are stimulated by microtubule inhibitors. *J. Cell Sci.* 93:255–266.
5. Pletjushkina, O. J., A. M. Belkin, O. J. Ivanova, T. N. Oliver, J. M. Vasiliev, and K. A. Jacobson. 1998. Maturation of cell-substratum focal adhesions induced by depolymerization of microtubules is mediated by increased cortical tension. *Cell Adhes. Commun.* 5:121–135.
6. Rodriguez, O. C., A. W. Schaefer, C. A. Mandato, P. Forscher, W. M. Bement, and C. M. Waterman-Storer. 2003. Conserved microtubule-actin interactions in cell movement and morphogenesis. *Nat. Cell Biol.* 5:599–609.
7. Vasiliev, J. M., T. Omelchenko, I. M. Gelfand, H. H. Feder, and E. M. Bonder. 2004. Rho overexpression leads to mitosis-associated detachment of cells from epithelial sheets: a link to the mechanism of cancer dissemination. *Proc. Natl. Acad. Sci. USA.* 101:12526–12530.
8. Maddox, A. S., and K. Burridge. 2003. RhoA is required for cortical retraction and rigidity during mitotic cell rounding. *J. Cell Biol.* 160:255–265.
9. Bornens, M., M. Paintrand, and C. Celati. 1989. The cortical microfilament system of lymphoblasts displays a periodic oscillatory activity in the absence of microtubules: implications for cell polarity. *J. Cell Biol.* 109:1071–1083.
10. Pletjushkina, O. J., Z. Rajfur, P. Pomorski, T. N. Oliver, J. M. Vasiliev, and K. A. Jacobson. 2001. Induction of cortical oscillations in spreading cells by depolymerization of microtubules. *Cell Motil. Cytoskeleton.* 48:235–244.
11. Straight, A. F., A. Cheung, J. Limouze, I. Chen, N. J. Westwood, J. R. Sellers, and T. J. Mitchison. 2003. Dissecting temporal and spatial control of cytokinesis with a myosin II inhibitor. *Science.* 299:1743–1747.
12. Narumiya, S., T. Ishizaki, and M. Uehata. 2000. Use and properties of ROCK-specific inhibitor Y-27632. *Methods Enzymol.* 325:273–284.
13. Perret, E., A. Leung, A. Morel, H. Feracci, and P. Nassoy. 2002. Versatile decoration of glass surfaces to probe individual protein-protein interactions and cellular adhesion. *Langmuir.* 18:846–854.
14. Walmod, P. S., R. Hartmann-Petersen, S. Prag, E. L. Lepekhin, C. Röpke, V. Berezin, and E. Bock. 2004. Cell-cycle-dependent regulation of cell motility and determination of the role of Rac1. *Exp. Cell Res.* 295:407–420.
15. Ballestrem, C., B. Wehrle-Haller, and B. A. Imhof. 1998. Actin dynamics in living mammalian cells. *J. Cell Sci.* 111:1649–1658.
16. Sibarita, J.-B., H. Magnin, and J. R. De Mey. 2002. Ultra-fast 4D microscopy and high throughput distributed deconvolution. *IEEE Int. Symp. Biomedical Imaging*. 769–772.
17. Vasiliev, J. M. 1991. Polarization of pseudopodial activities: cytoskeletal mechanisms. *J. Cell Sci.* 98:1–4.
18. Malawista, S. E., and A. de Boisfleury Chevance. 1982. The cytokineplast: purified, stable, and functional motile machinery from human blood polymorphonuclear leukocytes. *J. Cell Biol.* 95:960–973.
19. Euteneuer, U., and M. Schliwa. 1984. Persistent, directional motility of cells and cytoplasmic fragments in the absence of microtubules. *Nature.* 310:58–61.
20. Verkhovsky, A. B., T. M. Svitkina, and G. G. Borisy. 1999. Self-polarization and directional motility of cytoplasm. *Curr. Biol.* 9:11–20.
21. Prescott, D. M., D. Myerson, and J. Wallace. 1972. Enucleation of mammalian cells with cytochalasin B. *Exp. Cell Res.* 71:480–485.
22. Keller, H., and P. Eggli. 1998. Protrusive activity, cytoplasmic compartmentalization, and restriction rings in locomoting blebbing Walker carcinosarcoma cells are related to detachment of cortical actin from the plasma membrane. *Cell Motil. Cytoskeleton.* 41:181–193.
23. Cunningham, C. C. 1995. Actin polymerization and intracellular solvent flow in cell surface blebbing. *J. Cell Biol.* 129:1589–1599.
24. Jungbluth, A., V. von Arnim, E. Biegelmann, B. Humbel, A. Schweiger, and G. Gerisch. 1994. Strong increase in the tyrosine phosphorylation of actin upon inhibition of oxidative phosphorylation: correlation with reversible rearrangements in the actin skeleton of *Dictyostelium* cells. *J. Cell Sci.* 107:117–125.
25. Raucher, D., and M. P. Sheetz. 2000. Cell spreading and lamellipodial extension rate is regulated by membrane tension. *J. Cell Biol.* 148:127–136.
26. Marcy, Y., J. Prost, M.-F. Carlier, and C. Sykes. 2004. Forces generated during actin-based propulsion: a direct measurement by micromanipulation. *Proc. Natl. Acad. Sci. USA.* 101:5992–5997.
27. Bretschneider, T., S. Diez, K. Anderson, J. Heuser, M. Clarke, A. Müller-Taubenberger, J. Köhler, and G. Gerisch. 2004. Dynamic actin patterns and Arp2/3 assembly at the substrate-attached surface of motile cells. *Curr. Biol.* 14:1–10.
28. Noireaux, V., R. M. Golsteyn, E. Friederich, J. Prost, C. Antony, D. Louvard, and C. Sykes. 2000. Growing an actin gel on spherical surfaces. *Biophys. J.* 78:1643–1654.
29. Sekimoto, K., J. Prost, F. Jülicher, H. Boukellal, and A. Bernheim-Groswasser. 2004. Role of tensile stress in actin gels and a symmetry-breaking instability. *Eur. Phys. J. E.* 13:247–259.

30. van der Gucht, J., E. Paluch, J. Plastino, and C. Sykes. 2005. Stress release drives symmetry breaking for actin-based movement. *Proc. Natl. Acad. Sci. USA.* 102:7847–7852.

31. Condeelis, J. S., and D. L. Taylor. 1977. The contractile basis of amoeboid movement V. The control of gelation, solation and contraction in extracts from *Dictyostelium discoideum*. *J. Cell Biol.* 74:901–927.

32. Conrad, P. A., K. A. Giuliano, G. Fisher, K. Collins, P. T. Matsudaira, and D. L. Taylor. 1993. Relative distribution of actin, myosin I, and myosin II during the wound healing response of fibroblasts. *J. Cell Biol.* 120:1381–1391.

33. Stossel, T. P. 1993. On the crawling of animal cells. *Science.* 260:1086–1094.

34. Munro, E., J. Nance, and J. R. Priess. 2004. Cortical flows powered by asymmetrical contraction transport PAR proteins to establish and maintain anterior-posterior polarity in the early *C. elegans* embryo. *Dev. Cell.* 7:413–424.

35. Bray, D., and J. G. White. 1988. Cortical flow in animal cells. *Science.* 239:883–888.

36. Kruse, K., J.-F. Joanny, F. Jülicher, J. Prost, and K. Sekimoto. 2004. Asters, vortices, and rotating spirals in active gels of polar filaments. *Phys. Rev. Lett.* 92:078101.

37. Trinkaus, J. P. 1973. Surface activity and locomotion of *Fundulus* deep cells during blastula and gastrula stages. *Dev. Biol.* 30:68–103.

38. Kimura, K., M. Ito, M. Amano, K. Chihara, Y. Fukata, M. Nakafuku, B. Yamamori, J. Feng, T. Nakano, K. Okawa, A. Iwamatsu, and K. Kaibuchi. 1996. Regulation of myosin phosphatase by Rho and Rho-associated kinase (Rho-kinase). *Science.* 273:245–248.

39. Krendel, M., F. T. Zenke, and G. M. Bokoch. 2002. Nucleotide exchange factor GEF-H1 mediates cross-talk between microtubules and the actin cytoskeleton. *Nat. Cell Biol.* 4:294–301.

40. Rogers, S. L., U. Wiedemann, U. Hacker, C. Turck, and R. D. Vale. 2004. *Drosophila* RhoGEF2 associates with microtubule plus ends in an EB1-dependent manner. *Curr. Biol.* 14:1827–1833.